Hysteresis loop shape of field-driven antiferromagnetic-ferromagnetic bilayers in experimental conditions

Svetislav Mijatović [1], Stefan Graovac [1], Djordje Spasojević [1], and Bosiljka Tadić [2,3]
[1] *Faculty of Physics, University of Belgrade, POB 44, 11001 Belgrade, Serbia*
[2] *Department of Theoretical Physics, Jožef Stefan Institute, Jamova 39, 1000 Ljubljana, Slovenia*
[3] *Complexity Science Hub Vienna, Metternichgasse 8, 1030 Vienna, Austria*

(Received 24 October 2024; revised 24 December 2024; accepted 20 January 2025; published 3 February 2025)

We simulate the field-driven magnetization reversal in the exchange-coupled antiferromagnetic-ferromagnetic bilayers, adapting the weakly disordered random-field Ising model to mimic experimental conditions with finite temperatures and driving field rates. Our results reveal how the theoretical ideal hysteresis loop shape with a central loop and side branches with multiple small steps corresponding to a given architecture at low temperatures and slow driving becomes systematically deformed under the combined impact of the elevated temperatures and driving speed. Notably, the loop becomes smoother with the number of steps diminishing as temperature and driving rate increase. The coercive field demonstrates a systematic increase with the driving rate, characterized by a power law with a universal exponent of $1/2$, known in random ferromagnets; meanwhile, the nonuniversal factor depends on temperature and the antiferromagnetic layer thickness. For moderate driving rates, the coercivity decays exponentially with the increasing temperature, and the central loop eventually collapses above the ferromagnetic transition temperature, with two side branches dominating the loop shape. However, for substantial driving rates, the incomplete spin relaxation before the new field is applied prevents such thermal effects, and the loop remains almost rectangular, with a step on each branch. Predicting a range of parameters where the desired hysteresis shape is stable, these findings can stimulate further experimental research and applications of the field-driven bilayers.

DOI: 10.1103/PhysRevB.111.064304

I. INTRODUCTION

Magnetic materials with hysteresis behavior have been in focus for a long time as memory materials where traditionally ferromagnetic materials were used [1]. In the latest developments of magnetic recording, called spintronics [2], the use of materials with antiferromagnetic ordering appears as advantageous to overcome intrinsic limitations of ferromagnets, in particular, in terms of density and speed [3]. In layered antiferromagnetic systems with typical 2-sublattice structure, for example, Mn2Au and similar materials, manipulation of magnetization by electrical current is enabled, utilizing spin-orbit coupling [4,5]. In this case, an alternating local field is created at each sublattice. Apart from its technical challenges, this mechanism is limited to the materials obeying the spin-orbit coupling. One of the recent breakthroughs in the field is the use of antiferromagnetic-ferromagnetic (AFM-FM) bilayers, which offers a promising alternative to manipulate antiferromagnetic order by an external magnetic field. Adding a ferromagnetic layer with a strong exchange coupling to the antiferromagnetic layer enables utilizing magnetization—the ferromagnetic order parameter, driven by the external magnetic field, to identify and manipulate antiferromagnetic spins; a comparison of both mechanisms supported by an experimental analysis has been done in the above-mentioned antiferromagnetic sample Mn2Au-Py with added permalloy layer [6].

Recently, many AFM-FM bilayers of different elements and architecture have been designed and investigated; see recent reviews, Refs. [7,8]. The materials employed have been extensively studied with various experimental methods, showing magnetic properties distinct from their three-dimensional (3D) and two-dimensional (2D) counterparts. It has been recognized that a critical factor in stabilizing a long-range magnetic order in bilayered materials is magnetic anisotropy [9,10]. The ongoing experimental investigations into 2D magnets and their heterostructures have uncovered numerous new phenomena, spurring further theoretical and numerical studies into AFM-FM bilayers [11–15]. Moreover, the coaction of antiferromagnetic and ferromagnetic interactions and the influence of disorder can lead to complex patterns of domain walls and their motion in bilayers [16–19]. The effects of the external magnetic field on AFM-FM heterostructures depends on the coupling between the layers and an interplay of physical parameters, such as driving-field rate and temperature, which differently influence both layers. In this context, predictive theoretical models are needed to investigate magnetization reversal under varied parameters [6,20–22].

Predicting the hysteresis behaviors of coupled AFM-FM bilayers with weak disorder remains theoretically challenging due to markedly different dynamical phenomena enabling the magnetization reversal in both layers and their interplay under varied coupling strength and external parameters. Precisely, the occurrence of domains and domain-walls motion under the external magnetic field provides jerky magnetization fluctuations during the reversal in disordered ferromagnets; these phenomena are associated with the out-of-equilibrium critical behavior on the hysteresis loop [23–25]. In contrast, the interpenetrating sublattices structure of antiferromagnetic samples,

for example, two sublattices in a cubic morphology, hinders domain expansion via domain wall motion; meanwhile, the spin reversal takes part in different spatially disconnected areas. Therefore, theoretical studies of the reversal process are vital for understanding the role of both FM and AFM layers in the emergent hysteresis behavior. This paper aims to show that theoretical concepts based on random-field Ising models are suitable for investigating these currently pressing questions in the physics of magnetic bilayers and their applications. Our primary goal is to perform extensive numerical simulations of field-driven AFM-FM bilayers to predict the properties of the hysteresis loop for experimentally varying parameters.

Theoretical investigations of the equilibrium and out-of-equilibrium critical behavior often used the ferromagnetic random-field Ising model (RFIM) as a prototypal model of disordered systems in the renormalization group [26,27] and numerical simulations [28–30] studies. The field-driven zero-temperature dynamics in RFIM on three-dimensional lattices have shown that magnetic disorder controls domain nucleation and the pinning of domain walls, leading to dynamic critical phenomena with scale-invariance and long-range temporal correlations [23,31]. The critical disorder and the associated scaling behavior of magnetization avalanches and the structure of Barkhausen noise in these systems have been investigated through extensive simulations and finite-size scaling and multifractal analyses [32,33]. A comprehensive review of developed computational techniques can be found in Ref. [30] and references therein. Since the FM layer is a thin disordered ferromagnetic material, it is important to emphasize that the phenomenon of out-of-equilibrium critical dynamics of hysteresis loops also exists in 2D RFIM systems and samples with finite thickness; see Refs. [34–36] and references therein, revealing a transition from 2D to 3D universality classes with increasing thickness. Furthermore, the observed scaling behavior of magnetization avalanches and Barkhausen noise in 2D RFIM systems have shown sensitivity to sample shape, lattice morphology, and the driving rate [37,38].

On the other hand, interest in the behavior of hysteresis loops in disordered antiferromagnetic systems has grown in view of their increasing application. Experimental research evidenced the staircaselike behavior of the hysteresis loop in the various antiferromagnetic systems and heterostructures, for example, in Refs. [39–41]. These results highlight the importance of the substrate's morphology in antiferromagnetic spin systems and suggest that the magnetic disorder in the AF layers may play a different role compared to the ferromagnetic layers. Theoretically, the appearance of weak random fields have been understood as the dominant type of disorder in antiferromagnetic systems, being induced by structural defects in the presence of the external field [42,43]. The out-of-equilibrium dynamic phenomena behind the magnetization reversal in antiferromagnetic systems have been much less explored. Recently, the Barkhausen-noise type fluctuations that accompany the transitions between different steps in the staircaselike hysteresis loops in AFM-FM heterostructures with weak random fields have been demonstrated in Ref. [20]. Furthermore, the simulations of field-driven Ising spin systems with antiferromagnetic interactions on complex geometric substrates (nanonetworks) [44,45] have shown the magnetization steplike changes and self-organized critical dynamics on hysteresis loop [46] induced by the geometric spin frustration without any magnetic disorder.

Building on the theoretical model of exchange-coupled antiferromagnetic-ferromagnetic bilayers with perpendicular magnetic anisotropy, introduced in Ref. [20], we expand the modeling approach to perform numerical investigations of field-driven magnetization-reversal processes in experimentally relevant conditions. Specifically, we conduct extensive numerical simulations of the field-driven spin-reversal dynamics on the hysteresis loop of AFM-FM heterostructures of different antiferromagnetic layer thicknesses, focusing on the impact of increased field driving rate in the interplay with a finite temperature on the hysteresis loop features. Our findings reveal how the increased driving rate of the external field and elevated temperature that prevent complete spin relaxation before the new field is applied can alter the hysteresis loop, compared to its "ideal" theoretical shape observed at low temperatures and slow (adiabatic) driving. For moderate driving rates, the central segment of the hysteresis loop is predominantly controlled by the ferromagnetic layer; meanwhile, the antiferromagnetic layer determines the features of side branches. At significant driving rates, however, a different pathway for magnetization reversal leads to a new form of hysteresis, characteristic of disordered antiferromagnetic materials, persisting over temperature variations and sampling. Our systematic analysis of hysteresis loop properties in a wide range of these parameters can help experimental research to set the parameters relevant to the desired loop properties.

II. MODEL AND SIMULATIONS

A. Antiferromagnetic-ferromagnetic bilayers model

We examine systems of Ising ± 1 spins located at a cubic lattice of base $L \times L$ forming coupled bilayers of antiferromagnetic (AF) and ferromagnetic (FM) materials with the respective thicknesses l_{AF} and l_F, and a weak random-field disorder. The system Hamiltonian is given by

$$\mathcal{H} = -\sum_{\langle ij\rangle\in\mathcal{F}} J_F\sigma_i\sigma_j - \sum_{\langle ij\rangle\in\mathcal{A}} J_A S_i S_j - \sum_{\langle ij\rangle: i\in\mathcal{F}, j\in\mathcal{A}} J\sigma_i S_j - \sum_{i\in\mathcal{F}} h_i\sigma_i - \sum_{j\in\mathcal{A}} h_j S_j - H(t)\left(\sum_{i\in\mathcal{F}}\sigma_i + \sum_{j\in\mathcal{A}} S_j\right), \quad (1)$$

where $\langle ij\rangle$ denotes nearest neighbors on the lattice, and $\mathcal{F}$ and $\mathcal{A}$ represent the FM and AFM layers with spins σ_i in ferromagnetic, and S_i in antiferromagnetic layers, respectively. The intralayer spin couplings are $J_F > 0$ in ferromagnetic and $J_A < 0$ in antiferromagnetic layers, while the interlayer coupling is J. The quenched random fields $\{h_i\}$ follow a zero-mean Gaussian distribution $\rho(h) = e^{-h^2/2R^2}/R\sqrt{2\pi}$ with standard deviation R as a measure of disorder in the system. The external field $H(t)$ varies over time to trace the hysteresis loop.

B. Simulations and sampling

We simulated the above-described bilayer spin systems with $J_F = 1$, $J = 0.5$, and $J_{AF} = -1$, using the lattice with

base (linear) size $L = 256$ and open boundaries along thickness and periodic boundaries in base directions. For each sample with quenched random fields, the simulations begin with all spins in the downward state $\sigma_i = -1$, $S_i = -1$, and a large negative external field $H(t = 0) = -H_{max}$ specified at the end of section. The field is then incrementally increased at each time step by a constant amount ΔH, and the spins are flipped with the flipping probability $p_i^{(\sigma)}$ for ferromagnetic spins

$$p_i^{(\sigma)} = \frac{\exp\left(-\sigma_i h_i^{\sigma,\mathrm{eff}}/T\right)}{\exp\left(-\sigma_i h_i^{\sigma,\mathrm{eff}}/T\right) + \exp\left(+\sigma_i h_i^{\sigma,\mathrm{eff}}/T\right)}, \quad (2)$$

determined by the effective local field for ferromagnetic spins

$$h_i^{\sigma,\mathrm{eff}} = \sum_{\langle j\rangle_i \in \mathcal{F}} J_F \sigma_j + \sum_{\langle j\rangle_i \in \mathcal{A}} J S_j + H + h_i\,, \quad (3)$$

and temperature T relative to the ferromagnetic transition temperature $T_c/J_F = 1$. Analogously, for antiferromagnetic spins, the flipping probability is

$$p_i^{(S)} = \frac{\exp\left(-S_i h_i^{\mathrm{S,eff}}/T\right)}{\exp\left(-S_i h_i^{\mathrm{S,eff}}/T\right) + \exp\left(+S_i h_i^{\mathrm{S,eff}}/T\right)}, \quad (4)$$

and their effective local field is given by

$$h_i^{\mathrm{S,eff}} = \sum_{\langle j\rangle_i \in \mathcal{A}} J_A S_j + \sum_{\langle j\rangle_i \in \mathcal{F}} J \sigma_j + H + h_i\,, \quad (5)$$

where for the sake of simplicity, we didn't show explicit dependency on time for the probabilities, effective fields, and external field in the above equations. Here, one should note that in the $T \to 0^+$ limit both flipping probabilities, $p_i^{(\sigma)}$ and $p_i^{(S)}$, tend to zero for the *field-stable spins* (i.e., the spins aligned with their effective local field) and, oppositely, tends to one for the *field-unstable spins* (i.e., the spins misaligned with their effective local field), so that the spin flipping is caused solely by the change in their effective local field.

Note that the first sum in Eqs. (3) and (5) are over the spin's nearest neighbors from the same layer, while the second one is over the nearest neighbors from another layer and is present only for spins at the boundary between the layers. The effective local fields are updated at each new time step and so are the flipping probabilities. Each spin is tested for flipping in each time step by the given probabilities, meaning that there is a possibility of thermal flipping for any spin in the system at any moment of discrete time. The flipping of spins proceeds in the form of avalanches causing changes in the system's magnetization per spin $M = (\sum_{i\in\mathcal{F}} \sigma_i + \sum_{j\in\mathcal{A}} S_j)/(N_\sigma + N_S)$, where N_σ and N_S refer to the number of ferromagnetic and antiferromagnetic spins, respectively. To complete the hysteresis loop, the external field is increased up to H_{max} and then decreased by the same ΔH down to $H = -H_{max}$. Regarding the value of H_{max}, it is chosen so that the corresponding flipping probabilities for all spins fall below $1/(N_\sigma + N_S)$ at $H = \pm H_{max}$. Therefore, one can take that all spins are field-stable if aligned upward at $H = H_{max}$, and conversely downward at $H = -H_{max}$. We use up to 1000 different disorder samples. The simulation details are provided in Appendix.

III. THE SHAPE OF THE HYSTERESIS LOOP AT FINITE TEMPERATURE AND DRIVING RATE

In the original reference [20], we have explored the behavior of AFM-FM bilayers using a similar model applying the dynamical rules where only field-unstable spins (i.e., the spins aligned against their effective local field) could flip. These rules are appropriate for conditions with low temperatures and slow driving, allowing us to investigate the dependence of the hysteresis loop on system disorder, interlayer coupling, and the thickness of both layers. The current study focuses on the behavior of the hysteresis loop and coercive field under varying temperatures T and driving rates $\Omega \equiv \Delta H/\Delta t$; here, the time step is set to $\Delta t = 1$. The counterparts of these parameters are readily controlled in experiments, thus facilitating comparisons between numerical simulations and real-world observations. In this work, we used in all simulations the same weak disorder value $R = 0.05$; the impact of varying R and spin couplings J_F, J_{AF}, and J is studied in detail in Ref. [20].

In Fig 1, the 4×4 panels summarize representative shapes of the hysteresis loop emerging under the combined impact of the increasing driving rate (along the vertical direction) and the rising temperature (along the horizontal direction). The bottom-left panel shows a typical hysteresis loop for the given AFM-FM architecture obtained at very low temperatures and slow (nearly adiabatic) driving. Specifically, the antiferromagnetic layer predominantly shapes the loop tails, representing the initial and final sections of the loop with the steplike magnetization changes. Meanwhile, the ferromagnetic layer predominantly defines the central part of the loop. Within the AFM layer, spins gradually flip in smaller "portions," often comprising groups of spins with identical counts of previously flipped neighbors. Due to slight disorder, the primary factor distinguishing the values of the effective field h_i^{eff} at different lattice sites is the sum of neighboring spins, as the external field H remains equal for all spins. Consequently, spins with the same sum of the nearest-neighbor spin values will likely flip within the same avalanche once their effective field becomes positive. Conversely, in the FM layer, flipping a single spin can trigger an avalanche of flipped spin—a well-known mechanism in ferromagnetic materials [24,34]. Such collective spin flips in the ferromagnetic layer induces a significant jump at the coercive field value. This phenomenon elucidates the symmetric behavior of the loop around the point $(H, M) = (0, 0)$, with the value of the external field at zero magnetization referred to as the coercive field H_c. At lower temperatures and driving rates the hysteresis loops exhibit steps resembling a staircaselike pattern induced by flipping "portions" of spins in the AFM layer. These steps gradually diminish with increasing temperature and driving rate, and the loops become smoother. Similar hysteresis features are observed in experiments with different AF materials and layered structures, for example, in Refs. [39–41,47].

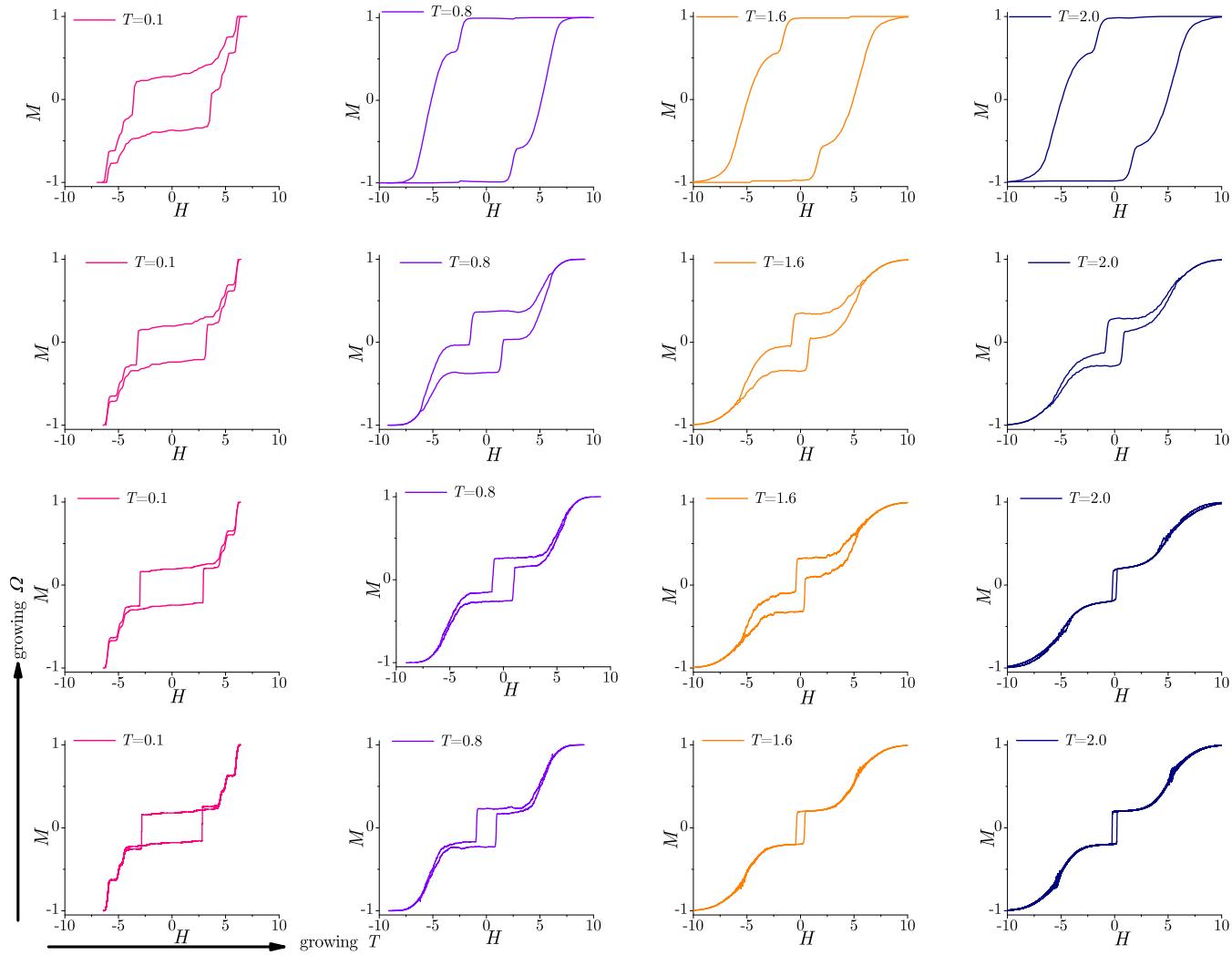

FIG. 1. The shapes of the hysteresis loop for the heterostructures with $\ell_F = 1$ and $\ell_{AF} = 4$ for varying driving rate $\Omega = 10^{-4}, 10^{-3}, 10^{-2}$, and $10^{-}1$ (bottom to top panels) and the relative temperature $T = 0.1$, 0.8, 1.6, and 2.0 (left to right panels); see text. The error bars, given by the standard deviations of the distribution of $M(H)$ values obtained in 1000 simulations with different random field configurations, are small (e.g., 0.002 for $T = 0.5$ and $\Omega = 10^{-1}$ case) and are not graphically presented.

In particular, when Ω is increased from extremely slow ($\Omega = 10^{-4}$ in the bottom panel) to fast driving ($\Omega = 10^{-1}$ in the top panel), meanwhile keeping the low temperature $T = 0.1$, the first column in Fig. 1 shows the systematical broadening of the side branches in the vertical direction and at the same time the width of the central loop grows (increasing H_c) with the driving rate. The magnetization steps remain recognizable despite the smoothing by the increased driving rate. Meanwhile, the increasing temperature induces dramatic effects even at prolonged driving by shrinking the central loop (decreasing H_c) and washing out the steplike structure in the side branches of the loop. In the remaining columns of Fig. 1, the results corresponding to three temperatures, $T = 0.8$, $T = 1.6$, and T = 2.0 are shown, which are below, above, and significantly above T_c, respectively. In this temperature range, the thermal activation for the spin-flipping probability p_i in Eqs. (2)–(4) increases compared to the low-temperature case, where the field-induced flipping dominates. Ultimately, the hysteresis loop would collapse at high temperatures and low driving rates, indicating the thermal destruction of all loop-related effects in agreement with experimental results, for example, see Refs. [7,48]. The increasing driving rates combat these thermal effects by broadening the loop side branches and increasing the width of the central loop, as described above. For significant driving rates, however, incomplete spin relaxation before the new field is applied prevents such thermal effects, thereby activating a new pathway for magnetization reversal; this leads to a new nearly rectangular loop shape with one step on each branch, resembling hysteresis loops observed in a weakly disordered antiferromagnetic material $PrVO_3$ in Ref. [40]. As shown in the top panels of Fig. 1, these forms of hysteresis appear stable to thermal variations and sampling. In the following section, we analyze the coercive field of AFM-FM bilayers, focusing on its nuanced dependencies on driving rate and temperature.

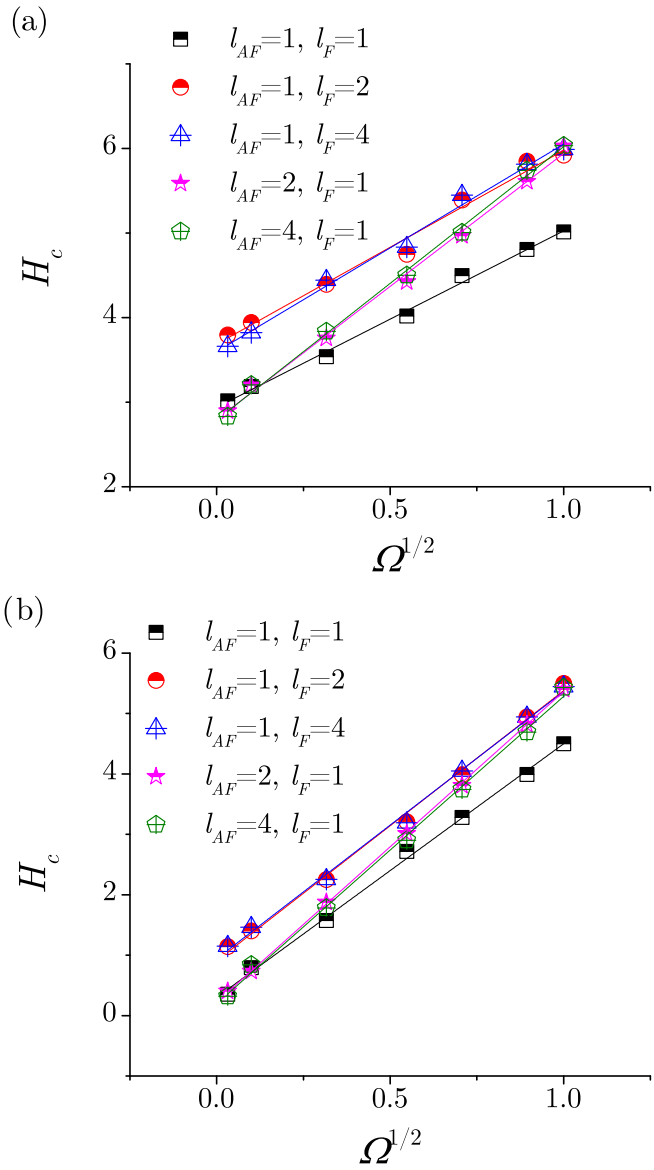

FIG. 2. The coercive field H_c plotted against the square root of the driving rate $\Omega^{1/2}$ for the AFM-FM heterostructures with different layer thicknesses, indicated in the legend, and two temperatures (a) $T = 0.1$ and (b) $T = 1.6$. The error bars are estimated as the standard deviation of the distributions of H_c values obtained in 1000 simulations with different random-field configurations ranging between 0.01 and 0.05, which is smaller than the symbols' size.

IV. REGULARITY IN THE COERCIVE FIELD DEPENDENCE ON DRIVING RATE AND TEMPERATURE

Determining the coercive field is of utmost importance in experimental investigations of magnetic materials [12,15,49]. In this context, the seminal work by Hoffman *et al.* [50] established the dependence of the coercive field on driving rate according to the square-root law. Our results shown in Figs. 2(a) and 2(b), considering a significant range of driving rates, demonstrate that $H_c = a\sqrt{\Omega}$ holds for the AFM-FM heterostructures, where the prefactor a remains independent on the driving rate, in agreement with Ref. [50]. The considered driving rates span from $\Omega = 10^{-3}$ to 1. Panel (a) of Fig. 2 showcases results at low temperatures, $T = 0.1$, while panel (b) illustrates the outcomes at $T = 1.6$. As Fig. 2 shows, this universal law applies at low temperatures and temperatures exceeding the ferromagnetic transition point. Furthermore, these results demonstrate how the temperature and the layer thickness impact the nonuniversal constant a. Notably, varying the AFM-FM architecture by changing the layer thicknesses results in two different slopes a in each temperature range. For example, for $T = 0.1$, two slopes in Fig. 2(a) determined (within error bars) are $a = 2.25 \pm 0.13$, corresponding to a group (I) of structures with a single AF layer $\ell_{AF} = 1$ and varied FM layer thickness $\ell_F \in [1, 4]$. Meanwhile, a larger value $a = 3.18 \pm 0.12$ corresponds to group (II) with varied AF layer thickness $\ell_{AF} \in [2, 4]$ and a single FM layer $\ell_F = 1$. A similar conclusion also holds for $T = 1.6$, with a larger coefficient $a = 4.32 \pm 0.16$ in the group (I) and $a = 5.14 \pm 0.12$ for the group (II); see the legend in Fig. 2(b).

The presented results reveal several significant features of the hysteresis behavior in the studied systems. Despite different initial points, the slopes of $H_c(\sqrt{\Omega})$ for systems in the group (I) with a solitary AFM layer remain indistinguishable (within the error bars). Furthermore, the coercive field values for the systems with a single FM layer consisting of the group (II) coincide. These observations confirm previous findings [20] that H_c in AFM-FM bilayers primarily varies based on ℓ_F. While the investigations in Ref. [20] are conducted at low driving rates, our current study covers a wide range of Ω, which allows us to observe the H_c dependence on the AF layer thickness ℓ_{AF}. In the low Ω limit, initial points of the curves in Figs. 2(a) and 2(b) roughly correspond to two distinct values of H_c set by the structure where ℓ_F or ℓ_{AF} equals one. Then, we can identify two different outcomes compared with the bottom curve, where both $\ell_F = \ell_{AF} = 1$. The middle curves with a larger slope a indicate the impact of the finite AF thickness $\ell_{AF} > 1$. Meanwhile, the two curves parallel to the bottom one but at a higher initial value suggest the growth of $H_c(\Omega)$ for $\ell_F > 1$ with $\ell_{AF} = 1$ primarily influenced by the FM layer. Decreasing the driving rate below a certain threshold renders the linear dependence of H_c on $\sqrt{\Omega}$ invalid. Below this threshold Ω_l, changes in H_c cease. The incremental changes in the external field are not sufficient to impact spin states within each discrete time step. Consequently, further reductions in Ω do not alter H_c. However, Ω_l varies with the system size, decreasing for larger systems due to the increased likelihood of small external field changes causing alterations in the system. The influence of temperature on the coercive field H_c represents a frequently studied aspect in experiments; see, for example, Refs. [10,47,51]. Our simulation results are depicted in Figs. 3(a) and 3(b), referring to two driving rates 10^{-3} and 0.5, respectively, for temperatures varied in the range $T \in [0.1, 2]$. Insets of Fig. 3 showcase the $H_c(T)$ dependence in linear scale, while the main figures adopt a lin-log scale. The system size and thickness mirror those in Fig. 2. Coercive field exhibits an exponential decay with temperature, $H_c \sim \mathrm{e}^{-bT}$, where the decay rate b remains independent of T, consistent with recent experimental findings on AFM and FM samples [47]. As the temperature rises, the likelihood of

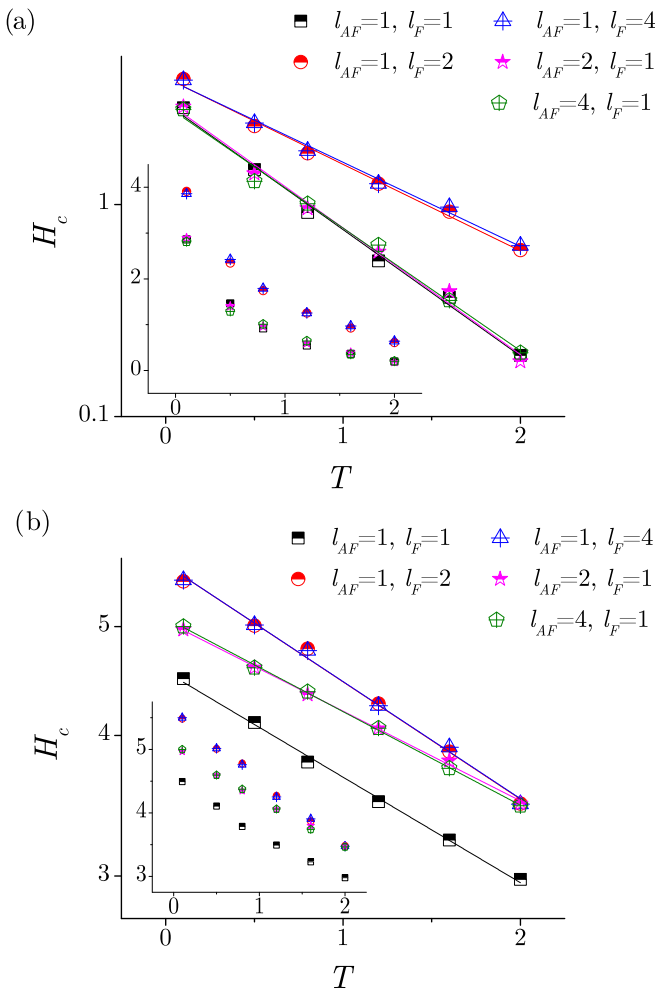

FIG. 3. The coercive field H_c plotted on lin-log scale against relative temperature T for the AFM-FM heterostructures of different thickness (indicated in the legend) and fixed driving rate (a) $\Omega = 10^{-3}$ and (b) $\Omega = 0.5$; Insets show the data on lin-lin scale. The error bars are similar as in Fig. 2.

flipping for the field-stable spins increases while decreasing for unstable spins [39]. The flipping probability for any spin stabilizes at $\frac{1}{2}$ for $T \to \infty$. Consequently, the increasing temperature leads to a higher average number of flipped spins at equivalent external field values, resulting in reduced H_c.

The decay rates b in $logH_c(T)$ vs T for two different groups (I) and (II) are found -0.60 ± 0.03 and -0.41 ± 0.02, for $\Omega = 10^{-3}$. Similarly, for $\Omega = 0.5$ the corresponding values for b are -0.10 ± 0.01 and -0.09 ± 0.01; cf. Fig. 3. While H_c decreases exponentially with T for all systems, the decay rate varies with the system's architecture. At lower driving rates, H_c declines more rapidly with temperature for systems with $\ell_F = 1$ compared to other cases indicated in the legend. This feature arises from substantial spin flipping at higher temperatures, which can more easily trigger a big avalanche in a single-plane FM layer, compared to a thick layer. However, for higher driving rates, the decay of H_c with temperature remains consistent across different architectures, with apparent differences in slope, as seen in Fig. 3.

V. DISCUSSION AND CONCLUSIONS

We have studied the hysteresis behavior of weakly disordered antiferromagnetic-ferromagnetic bilayers driven by the external magnetic field. Specifically, adapting the random-field Ising model of the exchange-coupled bilayers introduced in Ref. [20], we have systematically investigated the hysteresis loop shape and the coercive field values under the combined impact of the driving-field rate and temperature, the parameters relevant to experimental conditions. We have fixed the coupling strength between the layers and kept the low disorder to mitigate its effects on the observed phenomena [20], and to facilitate a comparison with the available experimental results often referring to weakly disordered antiferromagnetic materials, for example, Ref. [40]. Meanwhile, the model rules are adapted to allow a wide variation of driving rates and change of temperature from very low to high relative to the transition temperature of the ferromagnetic layer.

Our main results are illustrated in Figs. 1–3. At low temperatures and slow (nearly adiabatic) driving, we observed a staircaselike hysteresis loops, with the number of steps associated with the bilayer architecture, defined by the antiferromagnetic and ferromagnetic layer thickness, in agreement with experimental findings, for example, reviewed in Refs. [39,41,47]. In particular, the appearance of a central loop is associated with the ferromagnetic layer, whereas the coupled antiferromagnetic layer primarily determines the part with both side branches with multiple small steps. The increasing driving rate and temperature effects wash out the steplike magnetization changes, resulting in a smoother loop. However, their mutual impacts compete, leading to exciting deformations of the hysteresis loop shape and its properties, as shown by the representative cases in Fig. 1. On one side, the increased driving field rate tends to broaden the side branches and increase the width of the central loop. On the other side, increased temperature leads to the shrinking of the loop in each of its elements; with a slow field-driving rate, the loop eventually collapses at temperatures well above the transition point. Competition between these effects predominantly manifests in the magnetization reversal within the ferromagnetic layer, which occurs at H_c via a spanning avalanche (i.e., the avalanche that spreads along at least one of the base dimensions). These concurrent mechanisms depend on the relation between the time scale of thermal fluctuations and the field driving relative to the avalanche propagation time [52]. When driving is slow enough and at low temperatures, the spin flipping is primarily influenced by the orientation of neighboring spins and the external field. As the temperature rises, the probability of thermal spin flipping increases, potentially leading to diverse effects. On one side, the possibility of spins flipping at lower external field values facilitates the propagation of an avalanche that flips nearly all spins in the FM layer [53]. Conversely, thermal flipping may hinder the appearance of a large avalanche in the FM layer by reverting spin state, thereby obstructing the avalanche propagation. What mechanism will prevail depends on the driving rate, with higher rates favoring the appearance of large avalanches, as the external field increases faster than the temperature can compensate for spin flipping. Consequently, the coercive field decreases with temperature, but the decrease rate is lower for

more significant driving speeds. Eventually, when the driving speed is large such that the avalanche-triggering field is increased at the same scale as the avalanche propagates, the effects of thermal fluctuations are washed out; the situation results in the characteristic hysteresis shape shown in the three top-right panels in Fig. 1. It should be noted that similar loop shapes were observed along b and c axis in the bulk antiferromagnetic material PrVO3 in Ref. [40], suggesting a potentially dominant role of the AF layer in the loop behavior at large driving rates.

Furthermore, our results in Figs. 2 and 3 elucidate the behavior of the coercive fields with varying temperatures and driving rates. Theoretical predictions and experimental evidence suggest that in magnetic materials subjected to constantly changing external fields, the coercive field increases proportionally to the square root of the driving rate [50]. Our simulations corroborated this behavior. Conversely, experiments have shown that coercive field exponentially decreases with temperature [47], a trend mirrored in our systems. Additionally, our results show how the prefactors a in the $H_c = a\sqrt{\Omega}$ law depend on the thickness of the antiferromagnetic layer, irrespective of temperature. However, for lower driving rates, the values of the coercive field are determined by the thickness of the ferromagnetic layer l_F, while for larger driving rates, both l_{AF} and l_F play a role. Regarding temperature, the decay rate b in $H_c(T)$ dependence on the thickness of the ferromagnetic layer remains consistent for lower driving rates, while for larger driving rates, the values of decay rate exhibit minimal variation across different system sizes.

In conclusion, our study provides novel findings in the realm of numerical modeling of antiferromagnetic-ferromagnetic bilayers, in particular, predicting the hysteresis properties in experimental conditions, which holds significance for further research and practical applications. The compelling agreement with previously published experimental results on similar structures suggests the usefulness of the established random-field Ising model with adapted field-driven dynamics. This theoretical approach paves the way for further investigations and applications of Ising-like models in the domain of AFM-FM bilayers.

ACKNOWLEDGMENTS

B.T. is supported by the Slovenian Research Agency under the Program No. P1-0044. S.M., S.G., and D.S. acknowledge the financial support from The Ministry of Science, Technological Development and Innovation of the Republic of Serbia (Grant No. 451-03-9/2021-14/200162).

APPENDIX: PROGRAM FLOW

We outline the workflow of the program used to simulate the presented results.

ALGORITHM 1. Program Flow: Field-driven spin dynamics in the disordered thin antiferromagnetic-ferromagnetic bilayers.

1: **INPUT:** Linear size L of square-lattice base, thicknesses l_{AF}, l_F of the antiferromagnetic and ferromagnetic layer, the field driving rate Ω, temperature T, and SEED to generate random fields; fix the intralayer couplings as $J_F = 1$ and $J_{AF} = -1$, interlayer coupling as $J = 0.5$, and disorder as $R = 0.05$;
2: Allocate the spins $\{s_i\}$ (for the sake of simplicity here both S_i and σ_i are denoted by s_i) and quenched random fields $\{h_i\}$ arrays with $N = L \times L \times (l_{AF} + l_F)$ elements; initialize empty array $spinsToFlip$;
3: Generate values of $\{h_i\}$ from the Gaussian distribution with standard deviation R and SEED;
4: **Simulation of the ascending branch of the hysteresis curve:**
5: Initialization: set all s_i to -1, set the system's magnetization $m = \sum_{i=1}^{N} \frac{s_i}{N}$ to -1, and set the external field H to the highest value for which all spins in the $s_i = -1$ state are field stable;
6: **while** $m < 1$ **do**
7: $H = H + \Delta H$;
8: **for all** sites i in the lattice **do**
9: Calculate the effective local field h_i^{eff}, see Eqs. (3) and (5), and the interaction energy $E_i = -h_i^{\text{eff}} s_i$;
10: Calculate its thermal probability of flipping p_i, see Eqs. (2) and (4);
11: **if** p_i suggests flipping of s_i **then**
12: Store site index i in the array $spinsToFlip$;
13: **end if**
14: **end for**
15: Flip all spins from $spinsToFlip$;
16: Register the number of upward and the number of downward flipped spins $n_{\pm}$; update the value of magnetization m;
17: Empty array $spinsToFlip$;
18: Sampling values H, m, $n_{\pm}$;
19: **end while**
20: **Simulation of the descending branch of the hysteresis curve:** Proceed with steps 6–21 but **while** $m > -1$ with the decreasing field $H = H - \Delta H$ to complete the loop;
21: Repeat steps 3–22 for different random-field configurations;
22: **END**

[1] R. L. Comstock, Review: Modern magnetic materials in data storage, J. Mater. Sci.: Mater. Electron. **13**, 509 (2002).
[2] V. Baltz, A. Manchon, M. Tsoi, T. Moriyama, T. Ono, and Y. Tserkovnyak, Antiferromagnetic spintronics, Rev. Mod. Phys. **90**, 015005 (2018).
[3] T. Jungwirth, J. Sinova, A. Manchon, X. Marti, J. Wunderlich, and C. Felser, The multiple directions of antiferromagnetic spintronics, Nat. Phys. **14**, 200 (2018).
[4] S. Fukami, C. Zhang, S. DuttaGupta, A. Kurenkov, and H. Ohno, Magnetization switching by spin–orbit torque in an

antiferromagnet–ferromagnet bilayer system, Nat. Mater. **15**, 535 (2016).

[5] S. Reimers, Y. Lytvynenko, Y. R. Niu, E. Golias, B. Sarpi, L. S. I. Veiga, T. Denneulin, A. Kovács, R. E. Dunin-Borkowski, J. Blasser, M. Klaui, and M. Jourdan, Current-driven writing process in antiferromagnetic Mn_2Au for memory applications, Nat. Commun. **14**, 1861 (2023).

[6] S. Jenkins, T. Wagner, O. Gomonay, and K. Everschor-Sitte, Revealing ultrafast domain wall motion in Mn_2Au through permalloy capping, Phys. Rev. B **109**, 224431 (2024).

[7] Y. Yao, X. Zhan, M. G. Sendeku, P. Yu, F. T. Dajan, C. Zhu, N. Li, J. Wang, F. Wang, and Z. Wang, Recent progress on emergent two-dimensional magnets and heterostructures, Nanotechnology **32**, 472001 (2021).

[8] C. Gong and X. Zhang, Two-dimensional magnetic crystals and emergent heterostructure devices, Science **363**, eaav4450 (2019).

[9] M. Gibertini, M. Koperski, A. F. Morpurgo, and K. S. Novoselov, Magnetic 2D materials and heterostructures, Nat. Nanotechnol. **14**, 408 (2019).

[10] B. Huang, M. A. McGuire, A. F. May, D. Xiao, P. Jarillo-Herrero, and X. Xu, Emergent phenomena and proximity effects in two-dimensional magnets and heterostructures, Nat. Mater. **19**, 1276 (2020).

[11] A. P. Malozemoff, Mechanisms of exchange anisotropy, J. Appl. Phys. **63**, 3874 (1988).

[12] D. Choo, R. W. Chantrell, R. Lamberton, A. Johnston, and K. O'Grady, A model of the magnetic properties of coupled ferromagnetic/antiferromagnetic bilayers, J. Appl. Phys. **101**, 09E521 (2007).

[13] J. Moritz, P. Bacher, and B. Dieny, Numerical study of the influence of interfacial roughness on the exchange bias properties of ferromagnetic/antiferromagnetic bilayers, Phys. Rev. B **94**, 104425 (2016).

[14] D. Lv, J. Loiu, F. Zhang, and D. Zhang, Magnetic behaviors of an antiferromagnetic/ferromagnetic bilayer in a time-dependent magnetic field, J. Mol. Graphics Model. **109**, 108032 (2021).

[15] Z. Li and S. Zhang, Coercive mechanisms in ferromagnetic-antiferromagnetic bilayers, Phys. Rev. B **61**, R14897(R) (2000).

[16] I. V. Shashkov, M. A. Lebyodkin, and V. S. Gornakov, Statistical and multifractal properties of Barkhausen jumps in exchange coupled antiferromagnetic/ferromagnetic bilayers, Solid State Phenom. **215**, 35 (2014).

[17] V. I. Nikitenko, V. S. Gornakov, A. J. Shapiro, R. D. Shull, K. Liu, S. M. Zhou, and C. L. Chien, Asymmetry in elementary events of magnetization reversal in a ferromagnetic/antiferromagnetic bilayer, Phys. Rev. Lett. **84**, 765 (2000).

[18] W. Zhang and K. M. Krishnan, Domain wall nucleation in epitaxial exchange-biased Fe/IrMn bilayers with highly misaligned anisotropies, J. Magn. Magn. Mater. **324**, 3129 (2012).

[19] A. D. Bang, F. K. Olsen, S. D. Sloetjes, A. Scholl, S. T. Retterer, C. A. F. Vaz, T. Tybell, E. Folven, and J. K. Grapstad, Magnetic domain formation in ultrathin complex oxide ferromagnetic/antiferromagnetic bilayers, Appl. Phys. Lett. **113**, 132402 (2018).

[20] S. Mijatović, S. Graovac, Dj. Spasojević, and B. Tadić, Tuneable hysteresis loop and multifractal oscillations of magnetisation in weakly disordered antiferromagnetic–ferromagnetic bilayers, Physica E **142**, 115319 (2022).

[21] S. W. Jang, M. Y. Jeong, H. Yoon, S. Ryee, and M. J. Han, Microscopic understanding of magnetic interactions in bilayer CrI_3, Phys. Rev. Mater. **3**, 031001(R) (2019).

[22] C.-L. Zou, D.-Q. Guo, F. Zhang, J. Meng, H.-L. Miao, and W. Jiang, Magnetization, the susceptibilities and the hysteresis loops of a borophene structure, Physica E **104**, 138 (2018).

[23] E. Vives and A. Planes, Hysteresis and avalanches in disordered systems, J. Magn. Magn. Mater. **221**, 164 (2000).

[24] G. Durin and S. Zapperi, The Barkhausen effect, The Science of Hysteresis **1**, 181 (2006).

[25] D. Spasojević, M. Marinković, D. Jovković, S. Janićević, L. Laurson, and A. Djordjević, Barkhausen noise in disordered striplike ferromagnets: Experiment versus simulations, Phys. Rev. E **109**, 024110 (2024).

[26] G. Parisi and N. Sourlas, Scale invariance in disordered systems: The example of the random-field Ising model, Phys. Rev. Lett. **89**, 257204 (2002).

[27] I. Balog, G. Tarjus, and M. Tissier, Criticality of the random field Ising model in and out of equilibrium: A nonperturbative functional renormalization group description, Phys. Rev. B **97**, 094204 (2018).

[28] J. P. Sethna, K. A. Dahmen, and O. Perković, Random-field Ising models of hysteresis, The Science of Hysteresis **1**, 107 (2006).

[29] S. Janićević, D. Knežević, S. Mijatović, and D. Spasojević, Scaling domains in the nonequilibrium athermal random field Ising model of finite systems, J. Stat. Mech. (2021) 013202.

[30] D. Spasojević, S. Janićević, S. Mijatović, and B. Tadić, Hysteresis-loop criticality in disordered ferromagnets–A comprehensive review of computational techniques, Comput. Model. Eng. Sci. **142**, 1021 (2025).

[31] S. Zapperi, P. Cizeau, G. Durin, and H. E. Stanley, Dynamics of a ferromagnetic domain wall: Avalanches, depinning transition, and the Barkhausen effect, Phys. Rev. B **58**, 6353 (1998).

[32] F. J. Perez-Reche and E. Vives, Finite-size scaling analysis of the avalanches in the three-dimensional Gaussian random-field Ising model with metastable dynamics, Phys. Rev. B **67**, 134421 (2003).

[33] B. Tadić, Multifractal analysis of Barkhausen noise reveals the dynamic nature of criticality at hysteresis loop, J. Stat. Mech. (2016) 063305.

[34] D. Spasojević, S. Janićević, and M. Knežević, Numerical evidence for critical behavior of the two-dimensional nonequilibrium zero-temperature random field Ising model, Phys. Rev. Lett. **106**, 175701 (2011).

[35] D. Spasojević, S. Mijatović, V. Navas-Portella, and E. Vives, Crossover from three-dimensional to two-dimensional systems in the nonequilibrium zero-temperature random-field Ising model, Phys. Rev. E **97**, 012109 (2018).

[36] B. Tadić, S. Mijatović, S. Janićević, D. Spasojević, and G. J. Rodgers, The critical Barkhausen avalanches in thin random-field ferromagnets with an open boundary, Sci. Rep. **9**, 6340 (2019).

[37] B. Tadić, Dynamical implications of sample shape for avalanches in 2-dimensional random-field Ising model with saw-tooth domain wall, Physica A **493**, 330 (2018).

[38] S. Mijatović, D. Jovković, and D. Spasojević, Nonequilibrium athermal random-field Ising model on hexagonal lattices, Phys. Rev. E **103**, 032147 (2021).

[39] H. Xu, F. Chen, B. Chen, F. Jin, C. Ma, and L. t. Xu, Synthetic antiferromagnets with steplike hysteresis loops and high-T_C based on all-perovskite $La_{0.7}Sr_{0.3}MnO_3$ superlattices, Phys. Rev. Appl. **10**, 024035 (2018).

[40] L. D. Tung, $PrVO_3$: An inhomogeneous antiferromagnetic material with random fields, Phys. Rev. B **72**, 054414 (2005).

[41] Q. Li, X. Yuan, L. Xing, and M. Xu, Magnetization and magneto-transport staircaselike behavior in layered perovskite Sr_2CoO_4 at low temperature, Sci. Rep. **6**, 27712 (2016).

[42] J. Cardy, Random-field effects in site-disordered Ising antiferromagnetss, Phys. Rev. B **29**, 505 (1984).

[43] S. Fishman and A. Aharony, Random field effects in disordered anisotropic antiferromagnets, J. Phys. C: Solid State Phys. **12**, L729 (1979).

[44] B. Tadić, K. Malarz, and K. Kułakowski, Magnetization reversal in spin patterns with complex geometry, Phys. Rev. Lett. **94**, 137204 (2005).

[45] B. Tadić, M. Andjelković, M. Šuvakov, and G. J. Rodgers, Magnetisation processes in geometrically frustrated spin networks with self-assembled cliques, Entropy **22**, 336 (2020).

[46] B. Tadić and N. Gupte, Hidden geometry and dynamics of complex networks: Spin reversal in nanoassemblies with pairwise and triangle-based interactions, Europhys. Lett. **132**, 60008 (2021).

[47] B. Chen, H. Xu, C. Ma, S. Mattauch, D. Lan, F. Jin, Z. Guo, S. Wan, P. Chen, G. Gao, F. Chen, Y. Su, and W. Wu, All-oxide–based synthetic antiferromagnets exhibiting layer-resolved magnetization reversal, Science **357**, 1294 (2017).

[48] Z. Fei, B. Huang, P. Malinowski, W. Wang, T. Song, J. Sanchez, W. Yao, D. Xiao, X. Zhu, A. F. May, W. Wu, D. H. Cobden, J.-H. Chu, and X. Xu, Two-dimensional itinerant ferromagnetism in atomically thin Fe_3GeTe_2, Nat. Mater. **17**, 778 (2018).

[49] V. Baltz, B. Rodmacq, A. Zarefy, L. Lechevallier, and B. Dieny, Bimodal distribution of blocking temperature in exchange-biased ferromagnetic/antiferromagnetic bilayers, Phys. Rev. B **81**, 052404 (2010).

[50] G. R. Hoffman, J. A. Turner, and H. K. Lachowicz, Variation of coercivity of magnetic materials with driving field, J. Appl. Phys. **34**, 2708 (1963).

[51] R. Sbiaa, I. Al-Omari, P. Kharel, M. Ranjbar, D. Sellmyer, J. Akerman, and S. Piramanayagam, Temperature effect on exchange coupling and magnetization reversal in antiferromagnetically coupled (Co/Pd) multilayers, J. Appl. Phys. **118**, 063902 (2015).

[52] F. J. Pérez-Reche, B. Tadić, L. Mañosa, A. Planes, and E. Vives, Driving rate effects in avalanche-mediated first-order phase transitions, Phys. Rev. Lett. **93**, 195701 (2004).

[53] S. Graovac, S. Mijatović, and Dj. Spasojević, Mechanism of subcritical avalanche propagation in three-dimensional disordered systems, Phys. Rev. E **103**, 062123 (2021).